

# Universal spin wave driven domain wall velocity in biaxial ferromagnets

Xinyi Jiao (焦心怡)<sup>1,2</sup>, X. S. Wang <sup>3</sup>, and Jin Lan (兰金) <sup>1,2,\*</sup>

<sup>1</sup>Center for Joint Quantum Studies and Department of Physics, School of Science, Tianjin University, 92 Weijin Road, Tianjin 300072, China

<sup>2</sup>Tianjin Key Laboratory of Low Dimensional Materials Physics and Preparing Technology, Tianjin University, Tianjin 300354, China

<sup>3</sup>School of Physics and Electronics, Hunan University, Changsha 410082, China



(Received 5 December 2023; accepted 1 March 2024; published 20 March 2024)

Spin wave and domain wall are two of basic excitations in magnetic systems, and their interplay is dictated by the competitions between underlying magnetic interactions. In biaxial ferromagnets with easy-axis and hard-axis anisotropies perpendicular to each other, both the spin wave precession and the domain wall rotation are suppressed in the hard-axis direction. Here we investigate the domain wall motion driven by the spin waves in a biaxial ferromagnet using a wave packet approach. We show that the domain wall acquires a universal velocity given by the product of spin wave group velocity and the square of spin wave amplitude in the third ordinary-axis direction. Such a universal domain wall velocity is a synergy of the angular and linear momentum transfer mechanisms, with their weights controlled by the spin wave ellipticity.

DOI: [10.1103/PhysRevB.109.094428](https://doi.org/10.1103/PhysRevB.109.094428)

## I. INTRODUCTION

Magnetic domain walls widely exist in all types of magnetic materials, and are of great interest for both scientific explorations and industrial applications [1–5]. A prominent utilization of magnetic domain wall is for nonvolatile information storage, as routinely implemented in the celebrated racetrack memory [6,7]. For complete exploitation of magnetic domain walls, a crucial ingredient is to drive domain wall motion via various external stimuli, including magnetic field [8,9], electric spin current [10,11], thermal gradient [12–15], as well as spin wave [16–18]. Sharing the common magnetic nature, the interplay between spin wave and domain wall is more appealing toward a purely magnetic information processing scheme [17,19,20].

Starting from the translational and rotational symmetries, the domain wall dynamics is routinely formulated by the linear [21–23] and angular [24–26] momentum transfer from spin wave, respectively. In ferromagnets, the domain wall is anticipated to move backward/forward by transmitting/reflecting spin wave [17,27]. Furthermore, in ferrimagnets and antiferromagnets, the direction of domain wall motion can be further manipulated by the spin wave polarization [22,28–31]. Moreover, the Dzyaloshinskii-Moriya interaction acts as an alternative source for either angular/linear momentum, and enriches the domain wall dynamics remarkably [32–34].

Despite above efforts, most of existing literatures are typically restricted to uniaxial magnets with only easy-axis anisotropy, in which the spin waves are supposed to be circularly polarized. However, hard-axis anisotropy inevitably exists in realistic magnetic materials, either in intrinsic form due to magnetocrystalline anisotropy [35,36], or in extrinsic form due to dipolar [37], piezomagnetic [38–40], or multiferroic [41] effects. In the presence of hard-axis anisotropy, the

rotational symmetry of domain wall is broken, and the spin wave becomes elliptically polarized [42], so that the magnetic dynamics becomes substantially complicated in biaxial magnets [43,44]. A thorough understanding that captures all these complications is thus crucial toward completely and precisely harnessing domain wall in a wider extent of magnetic materials and structures.

In this paper, we systematically investigate the spin wave driven domain wall motion in biaxial ferromagnet, in the presence of both easy-axis and hard-axis anisotropies. With the aid of spin wave packet, the domain wall is shown to experience fictitious electrostatic and Lorentz forces mediated by spin wave intensity and current, and develops a universal velocity due to the synergy of these two forces. Specifically, the domain wall velocity is given by the product of the spin wave group velocity and the square of spin wave amplitude in the third ordinary-axis direction, irrespective of the magnetic anisotropy combinations and damping. By establishing a force-momentum correspondence, we reveal that the universal domain wall velocity is a mixed form of linear and angular momentum transfer.

This paper is organized as follows. The basic formulations of domain wall and spin wave in biaxial ferromagnets are established in Sec. II. The domain wall dynamics induced by a spin wave packet, its connection between linear and angular momentum transfer, and the influence of magnetic damping, are presented in Sec. III, and the domain wall velocity induced by continuous spin waves is also systematically derived. In Sec. IV, micromagnetic simulations are carried out to verify the theoretical formulations. In Sec. V, a short discussion and conclusions are given.

## II. BASIC MODEL

### A. Magnetic dynamics in biaxial ferromagnet

Consider a magnetic wire extending along  $x$  axis, where the magnetization direction is denoted by the unit vector  $\mathbf{m}$ ,

\*Corresponding author: lanjin@tju.edu.cn

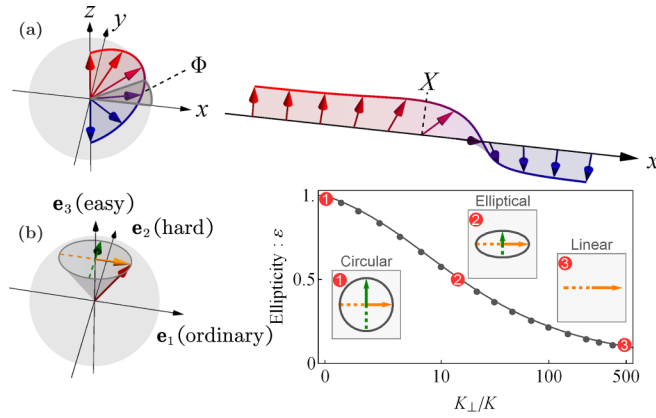


FIG. 1. Domain wall and spin wave in biaxial ferromagnets. (a) Magnetization profile of a domain wall. The arrows are for magnetization directions, and  $X$  and  $\Phi$  denote the central position and rotation angle, respectively. (b) Spin wave ellipticity as function of normalized hard-axis anisotropy  $K_{\perp}/K$  for wavevector  $k = 0.07 \text{ nm}^{-1}$ . The orange/green arrows are for spin wave components in ordinary axis  $\hat{\mathbf{e}}_1$  and hard axis  $\hat{\mathbf{e}}_2$ , respectively. The insets depict the spin wave precessions in circular/elliptical/linear fashion.

as depicted in Fig. 1(a). The magnetic dynamics is governed by the Landau-Lifshitz-Gilbert (LLG) equation

$$\dot{\mathbf{m}} = -\gamma \mathbf{m} \times \mathbf{h} + \alpha \mathbf{m} \times \dot{\mathbf{m}}, \quad (1)$$

where  $\dot{\mathbf{m}} \equiv \partial_t \mathbf{m}$ ,  $\gamma$  is the gyromagnetic ratio, and  $\alpha$  is the Gilbert damping constant. Here,  $\mathbf{h} = -(1/\mu_0 M_s) \delta u / \delta \mathbf{m}$  is the effective magnetic field acting on the magnetization  $\mathbf{m}$ ,  $\mu_0$  is the vacuum permeability, and  $M_s$  is the saturation magnetization. The energy density  $u$  of the biaxial magnetic wire is described by

$$u(\mathbf{m}) = \frac{\mu_0 M_s}{2} [A(\nabla \mathbf{m})^2 - K m_z^2 + K_{\perp} m_y^2], \quad (2)$$

where  $A$  is the exchange coupling constant,  $K$  is the easy-axis anisotropy in  $z$  axis, and  $K_{\perp}$  is the hard-axis anisotropy in  $y$  axis. For the convenience of narration in the following text, we notate  $z/x/y$  axis as easy/ordinary/hard-axis and  $\hat{\mathbf{x}}/\hat{\mathbf{y}}/\hat{\mathbf{z}}$  as  $\hat{\mathbf{e}}_{1/2/3}$ , respectively.

### B. Domain wall and spin wave

The ground state of the biaxial ferromagnet is either one of the homogeneous domains  $\mathbf{m} = \pm \hat{\mathbf{e}}_3$  along the easy axis. Upon the homogeneous domain, there are two typical excitations: the nonlinear domain wall with slow temporal varying magnetization  $\mathbf{m}_0$ , and the linear spin wave with fast temporal oscillating magnetization  $\mathbf{m}'$ . Before formulating their interaction, we establish the basic descriptions of domain wall and spin wave separately.

The domain wall generally takes the following Walker profile [8,45]:

$$\theta_0 = 2 \arctan \left[ \exp \left( \frac{x - X}{W} \right) \right], \quad \phi_0 = \Phi, \quad (3)$$

where  $\theta_0$  and  $\phi_0$  are polar and azimuthal angles of the domain wall magnetization  $\mathbf{m}_0$  about  $\hat{\mathbf{z}}$ . Here,  $W$  is the characteristic width of domain wall, and  $X$  and  $\Phi$  are the central position

and rotation angle, respectively. In biaxial magnets, the domain wall width is formulated by  $W = \sqrt{A/(K + K_{\perp} \sin^2 \Phi)}$  [8], which shrinks as the domain wall tilts away from the Néel configuration  $\Phi = 0$  at equilibrium. However, as we will show later, the domain wall width is hardly modified by the small rotation angle induced by spin wave ( $\Phi \ll 1$ ), hence is assumed to be constant  $W = \sqrt{A/K}$  throughout this paper. Because of the relatively fixed shape, the slow dynamics of domain wall can be parameterized by the evolution of minimal set of collective coordinates,  $\mathbf{m}_0(t) = \mathbf{m}_0[X(t), \Phi(t)]$ .

Meanwhile, the spin wave can be written as  $\mathbf{m}' = m_1 \hat{\mathbf{e}}_1 + m_2 \hat{\mathbf{e}}_2$ , where  $m_{1/2}$  are the ordinary/hard-axis components. In the linear regime, the spin wave dynamics is recast from LLG equation (1) to

$$-\dot{m}_1 = \gamma(-A \partial_x^2 + K + K_{\perp}) m_2, \quad (4a)$$

$$\dot{m}_2 = \gamma(-A \partial_x^2 + K) m_1. \quad (4b)$$

The monochromatic solution to Eq. (4) is

$$m_1 = c \sin(kx - \omega t), \quad m_2 = \tilde{c} \cos(kx - \omega t), \quad (5)$$

where  $c$  and  $\tilde{c}$  are the amplitudes in the ordinary and hard axis, and  $\omega$  and  $k$  are the angular frequency and wavevector obeying the quadratic dispersion relation  $\omega = \gamma \sqrt{(Ak^2 + K)(Ak^2 + K + K_{\perp})}$ . The rotational symmetry about the easy axis is broken by the hard-axis anisotropy  $K_{\perp}$  in Eq. (4), and thus the spin wave becomes elliptically polarized with

$$\varepsilon = \frac{\tilde{c}}{c} = \sqrt{\frac{Ak^2 + K}{Ak^2 + K + K_{\perp}}}, \quad (6)$$

where  $\varepsilon$  denotes the ellipticity [46], as depicted in Fig. 1(b).

In the basis of planar spin waves in Eq. (5), a localized spin wave packet can be constructed with Gaussian profile [47,48],

$$m_1 - \frac{i}{\varepsilon} m_2 = \frac{c}{\sqrt{4\pi}} \exp \left\{ -\frac{[x - \chi(t)]^2}{2\sigma^2} + ik[x - \chi(t)] \right\}, \quad (7)$$

where  $\chi$  is the central position, and  $\sigma$  is the characteristic width (see Appendix C). In the short-wavelength limit  $kW \ll 1$  of interest here, the width spreading in  $\sigma$  can be safely ignored, then the propagation of spin wave packet is equivalent to the kinematics of particle-like object with velocity

$$v \equiv \dot{\chi} = \frac{\partial \omega}{\partial k} = \frac{1 + \varepsilon^2}{\varepsilon} \gamma A k. \quad (8)$$

Moreover, the spin intensity and current carried by the spin wave packet in Eq. (7) are given by [15,34]

$$\rho = \int \frac{\langle m_1^2 + m_2^2 \rangle}{2} dx = \frac{(1 + \varepsilon^2) \sigma c^2}{4}, \quad (9a)$$

$$j = -\gamma A \int \left\langle m_1 \frac{\partial m_2}{\partial x} - m_2 \frac{\partial m_1}{\partial x} \right\rangle dx = \gamma \varepsilon \sigma c^2 A k, \quad (9b)$$

where  $\langle \dots \rangle$  represents the time averaging.

### III. DOMAIN WALL DYNAMICS INDUCED BY SPIN WAVE

In this section, we first investigate the domain wall dynamics driven by a spin wave packet, which has a clearer physical

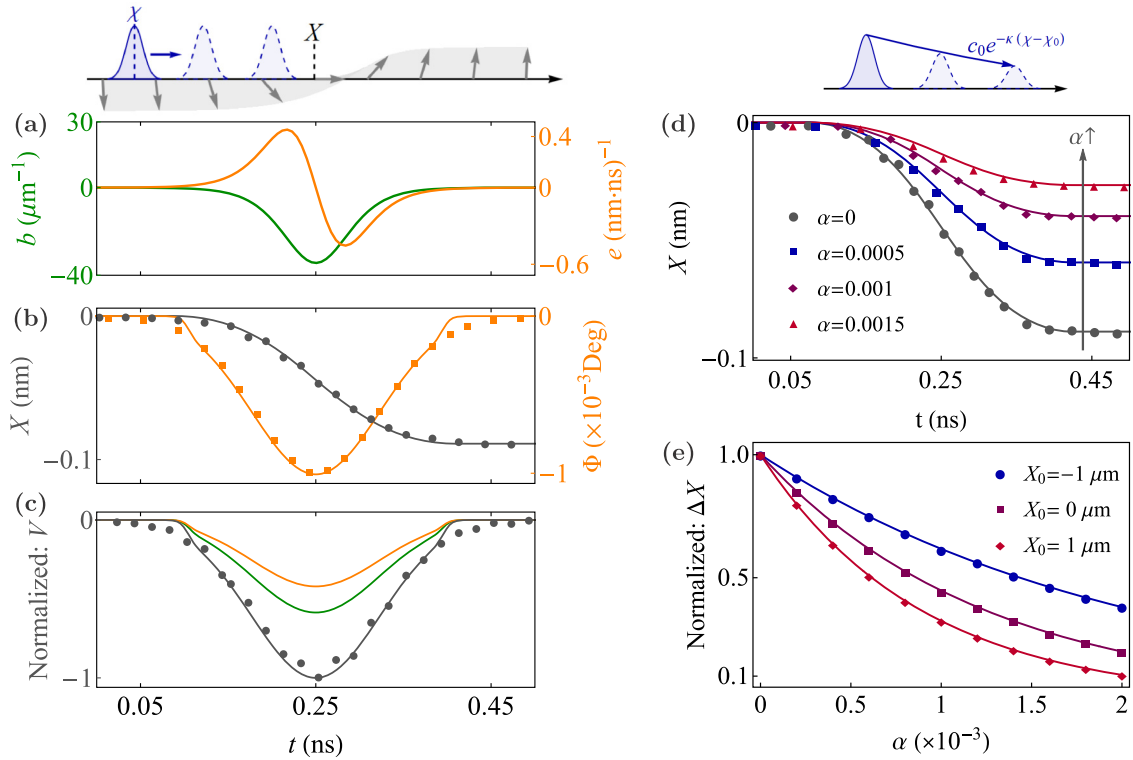


FIG. 2. Domain wall dynamics induced by a spin wave packet. (a) Spatial profile of the pseudo-electric (orange) and magnetic (green) fields. (b) Time evolution of central position (black) and rotation angle (orange) of the domain wall. (c) Time evolution of domain wall velocity (black) and its two subvelocities  $V_\rho$  (orange) and  $V_j$  (green). (d) Time evolution of the central position of domain wall under different magnetic damping constant  $\alpha$ . (e) Overall domain wall displacement  $\Delta X$  as function of magnetic damping. In (b)–(e), the dots are extracted from micromagnetic simulations, and the solid lines are calculated from theoretical models. The spin wave packet is excited at position  $x = -2.5 \mu\text{m}$ , and the magnetic damping is absent in (b) and (c). Small oscillations of domain wall position and velocity are hidden in dots with a large time step adopted here.

picture. With the underlying driving mechanism unambiguously identified, we then proceed to the case of continuous spin wave, that connects more closely to practical concerns.

### A. Dynamics induced by a spin wave packet

#### 1. Time evolution of domain wall

The intrinsic nonlinearity of magnetic interactions leads to the intimate interplay between spin wave and domain wall [36]. Specifically, the domain wall dynamics driven by a spin wave packet is governed by the following equations of motion (see Appendix D for detailed derivations):

$$2\dot{X} = jb + 2\gamma K_\perp W \Phi, \quad (10a)$$

$$2\dot{\Phi} = -\rho e, \quad (10b)$$

where  $e = -(2\gamma/\mu_0 M_s) \partial_x u(\mathbf{m}_0)$  and  $b = \mathbf{m}_0 \cdot (\partial_\Phi \mathbf{m}_0 \times \partial_x \mathbf{m}_0)$  are the pseudo-electric/magnetic fields induced by inhomogeneous domain wall magnetization [49–51]. Given Eq. (3), these two pseudofields are explicitly written as

$$e = -\frac{4\gamma K}{W} \text{sech}^2 \frac{\chi - X}{W} \tanh \frac{\chi - X}{W}, \quad (11)$$

$$b = -\frac{1}{W} \text{sech}^2 \frac{\chi - X}{W}, \quad (12)$$

which are antisymmetric and symmetric about the domain wall center, as plotted in Fig. 2(a).

We now consider the penetration of a wave packet through the domain wall, as schematically depicted above Fig. 2(a). According to the equation of motion (10b), the rotation angle  $\Phi$  is estimated first as

$$\Phi \approx - \int_{-\infty}^{\chi} \frac{\rho e}{2} \frac{d\chi'}{v} = -\frac{\gamma K}{v} \rho \text{sech}^2 \frac{\chi - X}{W}, \quad (13)$$

for which the magnitude of the rotation angle  $\Phi$  maximizes at the moment the spin wave packet reaches the domain wall center  $\chi = X$ . Above estimation is obtained by neglecting two minor factors: (i) the slight increment of spin wave velocity  $v$  within domain wall, and (ii) the small displacement of the domain wall itself. Note that the rotation angle always exists even when the hard-axis anisotropy is absent  $K_\perp = 0$ .

Furthermore, the domain wall velocity associated with Eq. (10a) is given by

$$V = V_\rho + V_j = - \left( \frac{\gamma^2 K K_\perp W}{v} \rho + \frac{1}{2W} j \right) \text{sech}^2 \frac{\chi - X}{W}, \quad (14)$$

where  $V_\rho$  and  $V_j$  are two subvelocities modulated by the same hyperbolic function despite distinct physical origins. The former is caused by the fictitious electrostatic force mediated by spin intensity  $\rho$ , while the latter is caused by the fictitious Lorentz force mediated by spin current  $j$ . Invoking Eq. (6) and inserting Eqs. (8) and (9), these two subvelocities are unified

to (see Appendix E for detailed derivations)

$$V_\rho = (1 - \xi)V, \quad V_j = \xi V, \quad (15)$$

where  $\xi = 2\varepsilon^2/(1 + \varepsilon^2)$  is the partition coefficient, and the total domain wall velocity is given by

$$V = -\frac{\sigma}{4W}c^2 v \operatorname{sech}^2 \frac{\chi - X}{W}. \quad (16)$$

Moreover, the overall displacement of the domain wall after the complete passage of a spin wave packet is described by

$$\Delta X \approx \int_{-\infty}^{\infty} V \frac{d\chi}{v} = -\frac{\sigma c^2}{2}, \quad (17)$$

which is simply controlled by the ordinary-axial amplitude  $c$  and the width  $\sigma$  of the spin wave packet.

## 2. Frame of momentum transfer

Above spin wave driven domain wall motion, analyzed via fictitious electromagnetic forces, can be reinterpreted under the frame of momentum transfer. Invoking the Noether theorem, the linear/angular momentum density for ferromagnetic system is formulated as [49,52]

$$\mathcal{P}_x = \cos\theta \frac{\partial\phi}{\partial x}, \quad \text{and} \quad \mathcal{S}_z = -\cos\theta, \quad (18)$$

where the former takes account of the surface area on the magnetic Bloch sphere subtended by the magnetization, and the latter is for  $z$  component of the magnetization, respectively. Other slightly different definitions of linear momentum density (e.g., Ref. [53]) may arise under different choices of gauge for the Wess-Zumino term in ferromagnets [54], but all physics are essentially the same.

Following Eq. (18), the linear/angular momenta of the spin wave packet in Eq. (7) are given by

$$p_x = \frac{\sigma c^2}{2} \varepsilon k, \quad (19a)$$

$$s_z = \frac{\sigma c^2}{4} (1 + \varepsilon^2) m_0^z. \quad (19b)$$

As the spin wave packet passes through the domain wall, its wavevector actually acquires a first-order correction  $\dot{k} = (1 + \varepsilon^2)e/(2\varepsilon)$  (see Appendix F for details). Above correction, along with the relation  $b = \partial_x m_0^z$ , then yield

$$\dot{p}_x = \frac{\sigma c^2}{2} \varepsilon \dot{k} = \frac{\sigma c^2}{4} (1 + \varepsilon^2) e = \rho e, \quad (20a)$$

$$\dot{s}_z = \frac{\sigma c^2}{4} (1 + \varepsilon^2) \frac{\partial m_0^z}{\partial x} \dot{\chi} = \rho v b. \quad (20b)$$

Equation (20a) takes account of the slight increment of linear momentum of spin wave packet within domain wall. After the full penetration of spin wave packet, its velocity along with its linear momentum restores to its original magnitudes, and the domain wall regains its linear momentum as well as its rotation angle. In contrast, Eq. (20b) represents an alternative form of continuity equation of the angular momentum  $\eta \dot{s}_z - \partial_x(jm_0^z) = 0$ , where  $\eta = j/\rho v = \xi^2/\varepsilon^2$  is the transmission efficiency of the angular momentum. The angular momentum is only perfectly transmitted ( $\eta = 1$ ) for circularly polarized

spin wave ( $\varepsilon = 1$ ), in the absence of the hard-axis anisotropy ( $K_\perp = 0$ ).

Meanwhile, the linear/angular momenta of the domain wall, in reference to the equilibrium configuration of  $\Phi = 0$  ( $X = 0$ ), are described by [27,36,52,55]

$$P_x = 2\Phi, \quad \text{and} \quad S_z = -2X. \quad (21)$$

The cross connections between linear/angular momentum with rotation angle (central position), originate from the gyroscopic nature of ferromagnetic dynamics.

Combining Eqs. (20) and (21), Eq. (10) is then rewritten as

$$\dot{P}_x = -\dot{p}_x, \quad \text{and} \quad \dot{S}_z = -\eta \dot{s}_z - 2\gamma K_\perp W \Phi. \quad (22)$$

Due to the preservation of translational symmetry, the linear momentum is simply transferred from spin wave to domain wall. Meanwhile, since the spin rotational symmetry is broken by hard-axis anisotropy, the angular momentum transfer involves two additional factors: (i) the angular momentum transmission is reduced by  $\eta$ ; (ii) the linear momentum is converted to angular momentum via the gyroscopic coupling. With above observations in Eq. (22), two subvelocities in Eq. (15) then naturally correspond to the linear/angular momentum transfer,

$$V_\rho = -\frac{\gamma K_\perp W \Delta p_x}{2}, \quad \text{and} \quad V_j = \frac{\eta \dot{s}_z}{2}, \quad (23)$$

and generally the domain wall velocity is a mixed transfer of both momenta.

The linear momentum transfer mechanism mediated by the gravity-like torque that underpins the subvelocity  $V_\rho$  is distinct from the mechanism in other literatures that is mediated by the entropic torque [13,15,56,57] (see Appendix D for explicit expressions of these two torques): (i) The gravity-like torque is caused by the reduction of magnetic texture energy by magnons, while the entropic torque (or pressure-like torque) originates from the nonadiabaticity of magnetization precessions [15,34]; and (ii) the linear momentum transfer is only temporary during the spin wave penetration here [48], but is permanent for the case of entropic torque.

## 3. Influence of magnetic damping

When magnetic damping is present  $\alpha \neq 0$ , the spin wave dispersion becomes  $(\varepsilon + i\alpha)\omega = \gamma[A(k + i\kappa)^2 + K]$ , where  $\kappa$  is the imaginary wavevector. For spin wave excited at fixed point  $x_0$  with amplitude  $c_0$  and angular frequency  $\omega$ , the spin wave decays as propagation with  $c = c_0 e^{-\kappa(x-x_0)}$  and  $\kappa = \alpha\omega/(2\gamma Ak)$ . Similarly, the spin intensity  $\rho$  and current  $j$  of a spin wave packet also decay with  $e^{-2\kappa x}$  in space or  $e^{-\beta t}$  in time with  $\beta = 2\kappa v$  the dissipation rate.

With the inclusion of magnetic dissipation, the domain wall dynamics triggered by the passage of a spin wave packet is then extended from Eq. (10) to

$$\dot{X} - \alpha W \dot{\Phi} = \gamma K_\perp W \Phi + \frac{j b}{2}, \quad (24a)$$

$$\dot{\Phi} + \frac{\alpha}{W} \dot{X} = -\frac{\rho e}{2}, \quad (24b)$$

where the domain wall motion and rotation are hybridized together. The dynamics of rotation angle  $\Phi$  in Eq. (24) can

be reorganized to

$$\dot{\Phi} + \alpha\gamma K_{\perp}\Phi = -\frac{\rho e}{2} - \frac{\alpha}{2W}jb, \quad (25)$$

where the dissipative corrections arise at both sides in comparison to Eq. (10b). Above equation (25) can be further transformed to

$$\dot{\Phi} + (1 - \xi)\beta\Phi = (\dot{\Phi}_0 - \xi\beta\Phi_0)e^{-\beta t}, \quad (26)$$

where  $\Phi_0$  is the rotation angle for the undamped case in Eq. (13). Therefore, the rotation angle  $\Phi$  in Eq. (26), and further the velocity  $V$  in Eq. (24a), are simply subjected to a common dissipation factor  $e^{-\beta t}$  in time, or alternatively  $e^{-2\kappa x}$  in space. Consequently, for a domain wall at initial position  $X_0$ , its displacement  $\Delta X$  is described by

$$\Delta X = -\frac{\sigma c^2}{2} = -\frac{\sigma c_0^2}{2}e^{-2\kappa(X_0 - \chi_0)}, \quad (27)$$

which maintains the same form as Eq. (17) but with active amplitude  $c$  now specifically taken at the domain wall center.

### B. Dynamics induced by continuous spin wave

As the reverse process of spin wave packet construction formulated in Eq. (7), continuous spin wave can be also decomposed into series of spin wave packets. When a planar spin wave is injected, equivalently multiple spin wave packets with total width  $\sigma = v\Delta t$  penetrate through the domain wall in a time interval  $\Delta t$ . According to Eqs. (17) and (27), the domain wall velocity during the passage of continuous spin wave is estimated to be

$$V = \frac{\Delta X}{\Delta t} = -\frac{c^2}{2}v, \quad (28)$$

which can be regarded as actuation relay of multiple spin wave packets. At the same time, the domain wall also acquires a constant angle during the passage of continuous spin wave  $\Delta\Phi = -2\gamma\rho KW/v$ , by performing similar procedures to Eq. (13).

Equation (28) is the central result of this paper, which reveals that the domain wall velocity in biaxial ferromagnets is simply given by the ordinary-axial amplitude square and the group velocity of spin wave, and is irrelevant to the spin wave ellipticity  $\varepsilon$  or the magnetic damping  $\alpha$ . Hence, the universal velocity in Eq. (28) applies for all combinations of easy-axis anisotropy  $K$  and hard-axis anisotropy  $K_{\perp}$ , by collecting partial yet complementary contributions from  $V_{\rho}$  and  $V_j$  as formulated in Eq. (15) via adjusting the partition coefficient  $\xi$ .

## IV. NUMERICAL RESULTS

The spin wave driven domain wall dynamics formulated in the preceding sections is further investigated via two types of numerical tools in parallel: (i) micromagnetic simulations using MuMax3 package [58] based on LLG equations (1); and (ii) numerical calculations by solving equations of motion in (10) and (24).

In micromagnetic simulations, we consider a one-dimensional wire along  $x$  direction with exchange coupling constant  $A = 3.28 \times 10^{-11}$  A m,  $z$ -easy-axis anisotropy

$K = 3.88 \times 10^4$  A m $^{-1}$ , and  $y$ -hard-axis anisotropy  $K_{\perp}/K = 50$  by default. The demagnetization field is turned off to purify the effect of the anisotropy and the spin wave. The total length of the wire is 10  $\mu\text{m}$  with mesh size of 2 nm. A domain wall is initially placed at the center of the wire with  $X_0 = 0$  nm, and its temporal and spatial evolutions are monitored. Absorbing boundaries of length 0.5  $\mu\text{m}$  are set at both ends by linearly increasing the damping constant from  $\alpha \approx 0$  in the bulk to  $\alpha = 0.35$  at the ends of the wire, to remove redundant spin waves reaching boundaries and prevent their reflections.

### A. Spin wave packet

The spin wave packet is prepared with the ordinary-axial amplitude  $c = 0.024$  and ellipticity  $\varepsilon = 0.64$ , the central wavevector  $k = 0.2$  nm $^{-1}$  and the characteristic width  $\sigma = 319$  nm, or in normalized form  $kW \approx 5.8$  and  $\sigma/W \approx 11$ . The choice of a relatively large spanning  $\sigma$  in simulations is to ensure that spin wave packet maintains a roughly fixed shape during propagation (see Appendix C).

For a negligible damping  $\alpha = 0$ , the time evolutions of the rotation angle  $\Phi$  and central position  $X$  extracted from simulations are well captured by Eqs. (13) and (17), with the inclusion of smearing caused by the large spanning of spin wave packet, as plotted in Fig. 2(b). The maximal angle is  $\Phi \approx -0.001^\circ$ , and the maximal displacement is  $\Delta X \approx -0.09$  nm, indicating the small yet non-negligible domain wall dynamics triggered by a spin wave packet. The domain wall velocity  $V$  is further plotted in Fig. 2(c), where both two subvelocities  $V_{\rho}$  and  $V_j$  are indispensable ingredients, highlighting the crucial roles of both linear and angular momentum transfer. The division between two subvelocities are roughly  $V_{\rho} : V_j \approx 0.4 : 0.6$ , which coincides well with the partition coefficient  $\xi \approx 0.58$  estimated upon the ellipticity  $\varepsilon = 0.64$  according to Eq. (15).

When damping becomes remarkable  $\alpha \neq 0$ , the evolution of central position  $X$  of the domain wall still maintains similar behaviors, but in a smaller magnitude for larger magnetic damping, as plotted in Fig. 2(d). As summarized in Fig. 2(e), the overall domain wall displacement  $\Delta X$  exponentially decays as the damping constant  $\alpha$  increases with the decaying rate controlled by distance  $\chi_0 - X_0$  between spin wave source and domain wall, in line with formulation in Eq. (27).

### B. Continuous spin wave

The continuous spin wave is prepared with frequency  $f = 74$  GHz and ordinary-axial amplitude  $c = 0.0774$  in the period of [2, 8] ns by applying an oscillating magnetic field  $\mathbf{h}(t) = h_0 \cos(2\pi ft)\hat{\mathbf{x}}$  at [-400, -390] nm, where the magnitude of the exciting field is  $h_0 = 1.6 \times 10^5$  A/m. There is a small delay of  $\Delta t \approx 0.1$  ns for domain wall response, which is attributed to the finite time for spin wave to propagate from the source point to the domain wall center.

When damping is negligible  $\alpha = 0$ , the domain wall develops a constant backward velocity  $V \approx -9.6$  m/s during the period [2.1, 8.1] ns, as shown in the upper panel of Fig. 3(a). In addition, the domain wall stops immediately after the passage of all spin wave, despite its finite inertia endowed by the hard-axis anisotropy [48,60,61]. The finite velocity

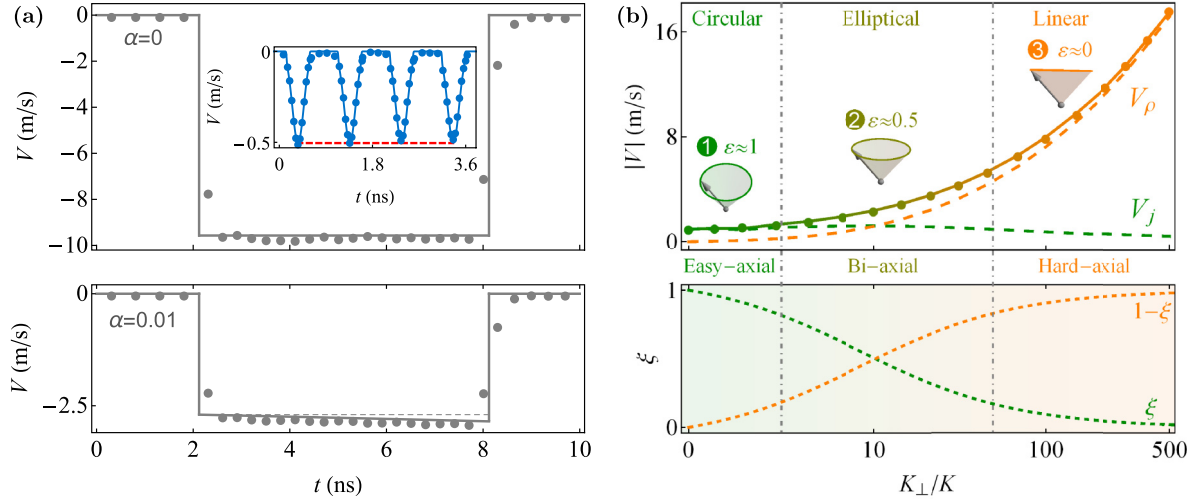


FIG. 3. Domain wall velocity induced by continuous spin wave. (a) Time evolution of domain wall velocity induced by a period of continuous spin wave. The upper panel is for  $\alpha = 0$ , and the lower panel is for  $\alpha = 0.01$ . The inset in upper panel is for the domain wall velocity driven by four consecutive spin wave packets. (b) Domain wall velocity  $V$  as function of normalized hard-axis anisotropy  $K_{\perp}/K$ . The orange/green dashed lines are for subvelocities  $V_{\rho}$  and  $V_j$  in the upper panel, and their weights  $1 - \xi$  and  $\xi$  in the lower panel. The dots are extracted from micromagnetic simulations, and the lines are calculated from theoretical models.

maintained only during the passage of continuous spin wave can be tracked back to the situations of multiple consecutive spin wave packets. Each time one spin wave packet passes, the domain wall develops a velocity peak, as depicted in inset of Fig. 3(a). In the limit of extremely dense distribution of spin wave packets, these discrete velocity peaks then merge together as a constant velocity plateau for continuous spin wave.

When damping is present  $\alpha \neq 0$ , the domain wall velocity is obviously reduced in comparison to the undamped case, as shown in the lower panel of Fig. 3(a). As the domain wall moves toward the source, the active spin wave amplitude increases, leading to a slight enhancement of the domain wall velocity in time.

The domain wall velocity is further investigated through series of simulations, where the hard-axis anisotropy  $K_{\perp}$  lies between 0 and  $500K$ . For convenience of comparisons, the spin wave wavevector is fixed to  $k = 0.07 \text{ nm}^{-1}$ , or in normalized form  $kW \approx 2$ , and the magnitude of the exciting magnetic field is fixed to  $h_0 = 3.98 \times 10^4 \text{ A/m}$ . As shown in Fig. 3(b), the domain wall velocity  $V$  in all simulations is well captured by the universal expression in Eq. (28) in the full range of anisotropies.

## V. DISCUSSIONS AND CONCLUSIONS

As demonstrated in Fig. 3(b), the overall velocity  $V$  is underpinned by two subvelocities  $V_{\rho}$  and  $V_j$  that evolve in opposite, albeit complementary, fashion. Based on contributions of two subvelocities, the whole range of hard-axis anisotropies roughly divides into three distinct regimes: easy-axial, biaxial, and hard-axial, with the main features summarized in Table I. In easy/hard-axial regime, the spin wave is circularly/linearly polarized, and the domain wall is purely driven by angular/linear momentum transfer. While for the biaxial regime lying in vast parameter range between these two extremes,

both the spin wave polarization and the domain wall driving mechanism are a mixture of two limits.

Given the ubiquitous hard-axis anisotropy in realistic magnetic materials and structures, the momentum transfer scenarios for spin wave driven domain wall deserve careful scrutiny. Obtrusively attributing the backward domain wall motion to angular momentum transfer, i.e., ignoring the influence of hard-axis anisotropy, may lead to faulty estimation of other magnetic parameters, especially during the experimental explorations.

In conclusion, we show that domain wall velocity in biaxial ferromagnets is universally given by the product of group velocity and ordinary-axial amplitude square of spin wave, irrespective of the underlying magnetic anisotropy and damping environment. Our paper offers insights into the rich role of hard-axis anisotropy in reconciling magnetic dynamics via breaking spin rotational symmetry.

## ACKNOWLEDGMENTS

This work is supported by National Natural Science Foundation of China (Grants No. 12374117 and No. 11904260) and Natural Science Foundation of Tianjin (Grant No. 20JCQNJC02020). X.S.W. acknowledges support from the Natural Science Foundation of China (NSFC) (Grants No. 11804045 and No. 12174093) and the Fundamental Research Funds for the Central Universities.

## APPENDIX A: SPIN WAVE UPON DOMAIN WALL

For spin wave  $\mathbf{m}'$  upon domain wall  $\mathbf{m}_0$ , the transverse condition  $\mathbf{m}' \cdot \mathbf{m}_0 = 0$  is satisfied everywhere in the small-amplitude limit  $|\mathbf{m}'| \ll 1$ . Hence, spin wave can be written as  $\mathbf{m}' = m_{\theta} \hat{\mathbf{e}}_{\theta} + m_{\phi} \hat{\mathbf{e}}_{\phi}$ , where  $\hat{\mathbf{e}}_{\theta/\phi}$  are two transverse directions about the background magnetization  $\hat{\mathbf{e}}_r \equiv \mathbf{m}_0$ .

TABLE I. Features of spin wave driven domain wall motion in three regimes of anisotropies.

Anisotropy	Parameters	Ellipticity $\varepsilon$	Partition coefficient $\xi$	Force	Momentum	Refs.
Easy-axial	$K_{\perp} \sim 0$	1	1	Lorentz	Angular	[24,25,34,59]
Biaxial	$K_{\perp} \sim K + Ak^2$	$\sqrt{\frac{Ak^2+K}{Ak^2+K+K_{\perp}}}$	$\frac{2\varepsilon^2}{1+\varepsilon^2}$	Electromagnetic	Mixed	This paper
Hard-axial	$K_{\perp} \gg K$	0	0	Electrostatic	Linear	[48]

Upon the domain wall profile in Eq. (3), the spin wave dynamics is recast from LLG equation (1) to

$$-\dot{m}_{\theta} = \gamma[-A\partial_x^2 + U(x) + K_{\perp}]m_{\phi}, \quad (\text{A1a})$$

$$\dot{m}_{\phi} = \gamma[-A\partial_x^2 + U(x)]m_{\theta}, \quad (\text{A1b})$$

where  $U(x) = K[1 - 2\text{sech}^2(x/W)]$  is effective potential induced by inhomogeneous magnetization within domain wall.

Equation (A1) hosts a series of reflectionless modes [62]

$$m_{\theta} = \frac{c}{\sqrt{1+k^2W^2}} \left[ kW \sin(kx - \omega t) + \cos(kx - \omega t) \tanh \frac{x}{W} \right], \quad (\text{A2a})$$

$$m_{\phi} = \frac{\tilde{c}}{\sqrt{1+k^2W^2}} \left[ kW \cos(kx - \omega t) - \sin(kx - \omega t) \tanh \frac{x}{W} \right]. \quad (\text{A2b})$$

Far away from the domain wall  $|x| \gg W$ , the effective potential flattens as  $U(x) \rightarrow K$ , and above wave solutions reduce to Eq. (5) with  $m_{\theta} \rightarrow \pm m_1$  and  $m_{\phi} \rightarrow m_2$ .

Above spin wave modes in Eq. (A2) can be approximated to

$$m_{\theta} \approx c \sin[kx - \omega t + \varphi(x)], \quad (\text{A3a})$$

$$m_{\phi} \approx \tilde{c} \cos[kx - \omega t + \varphi(x)], \quad (\text{A3b})$$

where  $\varphi(x) = \arctan[\tanh(x/W)/kW]$  is the position-dependent phase induced by the domain wall. Since only slight modification is introduced by domain wall in Eq. (A3), the spin wave in uniform domain in Eq. (5) is used throughout the main text for simplicity.

### APPENDIX B: DOMAIN WALL DYNAMICS WITHOUT SPIN WAVE

In the small-angle limit  $|\Phi| \ll 1$ , the domain wall dynamics is recast from LLG equation (1) to

$$\dot{X} - \alpha W \dot{\Phi} = \gamma K_{\perp} W \Phi, \quad (\text{B1a})$$

$$\dot{\Phi} + \frac{\alpha}{W} \dot{X} = 0, \quad (\text{B1b})$$

where the domain wall motion and rotation are coupled via the magnetic damping as well as the hard-axis anisotropy. Above Eq. (B1) can be rewritten as

$$\ddot{X} + \mu \dot{X} = 0, \quad \dot{\Phi} + \mu \Phi = 0, \quad (\text{B2})$$

where the domain wall motion and rotation share the same viscosity  $\mu = \alpha\gamma K_{\perp}/(1 + \alpha^2)$ . Beside the damping constant, the viscosity  $\mu$  is also modulated by hard-axis anisotropy.

Consider a domain wall with an initial configuration of  $X = 0$  and  $\Phi = \Phi_0 \neq 0$ , then the domain wall evolution is given by

$$X = \frac{W}{\alpha} \Phi_0 (1 - e^{-\mu t}), \quad \Phi = \Phi_0 e^{-\mu t}, \quad (\text{B3})$$

where the maximal displacement of domain wall is independent of the hard-axis anisotropy. The time evolutions of domain wall for an initial angle of  $\Phi_0 = 1^\circ$ , in micromagnetic simulations with fixed damping constant  $\alpha = 0.01$  yet different hard-axis anisotropies, are plotted in Fig. 4. As the hard-axis anisotropy increases, both the central position  $X$  and the rotation angle  $\Phi$  evolve faster, but the domain wall terminates at the same position  $X \approx 50.8$  nm.

### APPENDIX C: CONTINUOUS SPIN WAVE AND DISCRETE SPIN WAVE PACKETS

The magnetization profiles of continuous spin wave and discrete spin wave packets are schematically shown in Figs. 5(a) and 5(b), respectively. The inequivalence between magnetization oscillations  $m_{1/2}$  in the ordinary/hard axis, as depicted in the inset of Fig. 5(b), is due to the existence of hard-axis anisotropy. Apparently, by making the distribution of spin wave packets extremely dense, a continuous spin wave

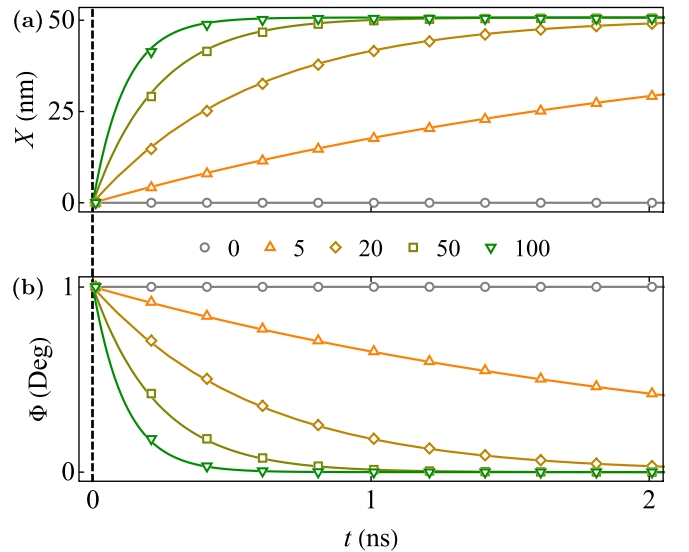


FIG. 4. Time evolution of an initially tilted domain wall under different hard-axis anisotropies. The initial rotation angle is set to  $\Phi_0 = 1^\circ$ , and the damping constant is set to  $\alpha = 0.01$ . The dots are extracted from micromagnetic simulations, and the lines are calculated from theoretical models.

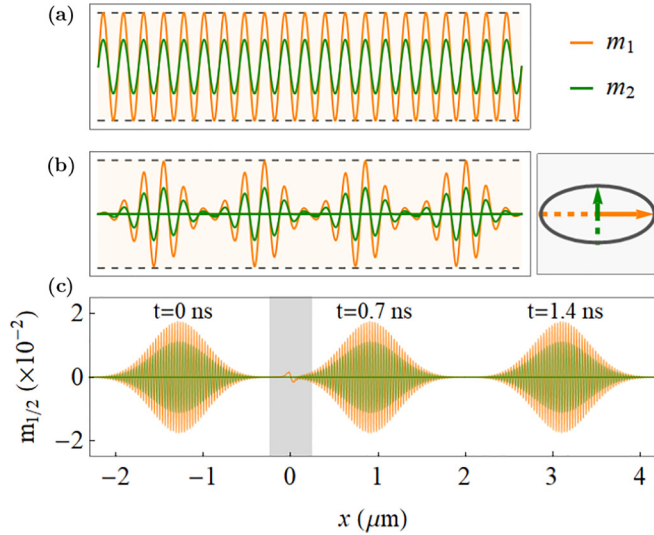


FIG. 5. Spin wave in biaxial ferromagnets. Schematics of magnetization profile of (a) continuous spin wave and (b) discrete spin wave packets. (c) Three time positions of a spin wave packet passing through the domain wall, where the lines are extracted from micromagnetic simulation, and the shaded region represents the domain wall. In all plots, the orange/green lines represent the magnetization  $m_{1/2}$  along the ordinary/hard-axial direction, respectively.

is then restored. Therefore, one can treat continuous spin wave as a train of spin wave packets.

The penetration of a spin wave packet through a domain wall in micromagnetic simulation is plotted in Fig. 5(c). No obvious spreading of spin wave packet is observed in the whole penetration process of duration 1.4 ns. Therefore, the propagation of a spin wave packet takes close analogy to a particle-like object in the short-wavelength limit. Moreover, before and after penetrating the domain wall, the amplitude and velocity of the spin wave packet remain unchanged, which indicates that the change of its linear momentum is not permanent [48].

#### APPENDIX D: MAGNONIC TORQUE EXERTED BY SPIN WAVE

A powerful approach to formulate the action exerted by the fast oscillating spin wave on the background magnetization is the magnonic torque [15,34,59,63].

Dividing the total magnetization into domain wall part  $\mathbf{m}_0$  and spin wave part  $\mathbf{m}'$ , the total magnetization can be expressed as

$$\mathbf{m} \approx \left(1 - \frac{\mathbf{m}' \cdot \mathbf{m}'}{2}\right) \mathbf{m}_0 + \mathbf{m}', \quad (\text{D1})$$

where the reduction of domain wall magnetization  $\mathbf{m}_0$  is employed to enforce the unity condition  $|\mathbf{m}| = 1$ . According to above partition scheme, the LLG equation (1) is transformed to [34]

$$\dot{\mathbf{m}}_0 - \alpha \mathbf{m}_0 \times \dot{\mathbf{m}}_0 = -\gamma \mathbf{m}_0 \times \mathbf{h}(\mathbf{m}_0) + \boldsymbol{\tau}, \quad (\text{D2})$$

where  $\boldsymbol{\tau}$  is the magnonic torque exerted by spin wave  $\mathbf{m}'$ . After time averaging, the magnonic torque is explicitly described by

$$\boldsymbol{\tau} = J \partial_x \mathbf{m}_0 + 2\varrho [\mathbf{m}_0 \times \gamma \mathbf{h}(\mathbf{m}_0)], \quad (\text{D3})$$

where the first term is the spin-transfer torque mediated by the spin flux  $J$ , and the second term is gravity-like torque mediated by the spin density  $\varrho$ . Considering the specific form of the wave packet of interest here, a third pressure-like torque (also known as the entropic torque [13,15,56,57])  $\gamma A \partial_x \varrho (\mathbf{m}_0 \times \partial_x \mathbf{m}_0)$  is ignored. The spin density and flux carried by spin wave in Eq. (D3) read

$$\varrho \equiv \frac{\langle \mathbf{m}' \cdot \mathbf{m}' \rangle}{2}, \quad J \equiv \gamma A \langle \partial_x \mathbf{m}' \times \mathbf{m}' \rangle \cdot \mathbf{m}_0, \quad (\text{D4})$$

where  $\langle \dots \rangle$  represents the time averaging.

For spin wave packet localized around its central position  $\chi$ , above two quantities are rewritten as

$$\varrho = \rho \delta(x - \chi), \quad J = j \delta(x - \chi), \quad (\text{D5})$$

where  $\rho$  and  $j$  are spin intensity and current following Eq. (9). In the meantime, in collective coordinates  $X$  and  $\Phi$ , the domain wall evolution is captured by  $\mathbf{m}_0(t) = \mathbf{m}_0[X(t), \Phi(t)]$ . Left multiplying  $\mathbf{m}_0 \times \partial_{X/\Phi} \mathbf{m}_0$  and integrating in the whole magnetic wire, the modified LLG equation (D2) is then transformed to generalized Thiele equation (10) in the main text.

#### APPENDIX E: DERIVATIONS OF THE SUBVELOCITIES OF DOMAIN WALL

Equation (6) can be recast to following form:

$$\frac{K_{\perp}}{Ak^2} \approx \frac{K_{\perp}}{Ak^2 + K} = \frac{1 - \varepsilon^2}{\varepsilon^2}, \quad (\text{E1})$$

where the short-wavelength approximation  $Ak^2 \gg K$  is used. Based the relation in Eq. (E1), the spin wave velocity in Eq. (8) and the spin intensity in Eq. (9a), the coefficient of  $V_{\rho}$  in Eq. (14) is then given by

$$\begin{aligned} \frac{\gamma^2 K K_{\perp} W}{v} \rho &= \frac{\gamma^2 A K_{\perp}}{v^2} \frac{v \rho}{W} \\ &= \frac{K_{\perp}}{Ak^2} \frac{\varepsilon^2}{(1 + \varepsilon^2)^2} \frac{v \rho}{W} \\ &= \frac{1 - \varepsilon^2}{1 + \varepsilon^2} \frac{\sigma}{4W} c^2 v. \end{aligned} \quad (\text{E2})$$

Meanwhile, invoking Eqs. (8) and (9b), the coefficient of  $V_j$  in Eq. (14) is rewritten as

$$\frac{1}{2W} j = \frac{1}{2W} \gamma \varepsilon \sigma c^2 A k = \frac{2\varepsilon^2}{1 + \varepsilon^2} \frac{\sigma}{4W} c^2 v. \quad (\text{E3})$$

Defining  $\xi = 2\varepsilon^2/(1 + \varepsilon^2)$ , Eqs. (E2) and (E3) then lead to Eq. (15) in the main text.

#### APPENDIX F: MOMENTUM VARIATION OF SPIN WAVE

In the short-wavelength limit (or WKB approximation), the local spin wave dispersion within the domain wall, following

Eq. (A1), is described by

$$\omega(x) = \gamma \sqrt{[Ak^2 + U(x)][Ak^2 + K_{\perp} + U(x)]}. \quad (\text{F1})$$

In configuration space  $\{x, k\}$ , the local dispersion  $\omega$  acts as the Hamiltonian of a particle-like object [50,64,65]. Invoking Eq. (6), the evolution of the wavevector  $k$  is

governed by

$$\begin{aligned} \dot{k} &= -\frac{\partial \omega}{\partial x} \approx -\frac{\gamma^2(2Ak^2 + K_{\perp} + 2K_0)}{2\omega} \frac{\partial U}{\partial x} \\ &= \frac{1 + \varepsilon^2}{2\varepsilon} e, \end{aligned} \quad (\text{F2})$$

which then leads to the correction in Eq. (20a).

- 
- [1] D. A. Allwood, G. Xiong, M. D. Cooke, C. C. Faulkner, D. Atkinson, N. Vernier, and R. P. Cowburn, Submicrometer ferromagnetic NOT gate and shift register, *Science* **296**, 2003 (2002).
- [2] D. A. Allwood, G. Xiong, C. C. Faulkner, D. Atkinson, D. Petit, and R. P. Cowburn, Magnetic domain-wall logic, *Science* **309**, 1688 (2005).
- [3] Z. Luo, T. P. Dao, A. Hrabec, J. Vijayakumar, A. Kleibert, M. Baumgartner, E. Kirk, J. Cui, T. Savchenko, G. Krishnaswamy *et al.*, Chirally coupled nanomagnets, *Science* **363**, 1435 (2019).
- [4] Z. Luo, A. Hrabec, T. P. Dao, G. Sala, S. Finizio, J. Feng, S. Mayr, J. Raabe, P. Gambardella, and L. J. Heyderman, Current-driven magnetic domain-wall logic, *Nature (London)* **579**, 214 (2020).
- [5] D. Kumar, T. Jin, R. Sbiaa, M. Kläui, S. Bedanta, S. Fukami, D. Ravelosona, S.-H. Yang, X. Liu, and S. N. Piramanayagam, Domain wall memory: Physics, materials, and devices, *Phys. Rep.* **958**, 1 (2022).
- [6] S. S. P. Parkin, M. Hayashi, and L. Thomas, Magnetic domain-wall racetrack memory, *Science* **320**, 190 (2008).
- [7] S. Parkin and S.-H. Yang, Memory on the racetrack, *Nat. Nanotechnol.* **10**, 195 (2015).
- [8] N. L. Schryer and L. R. Walker, The motion of 180° domain walls in uniform dc magnetic fields, *J. Appl. Phys.* **45**, 5406 (1974).
- [9] Y. Nakatani, A. Thiaville, and J. Miltat, Faster magnetic walls in rough wires, *Nat. Mater.* **2**, 521 (2003).
- [10] A. Thiaville, Y. Nakatani, J. Miltat, and N. Vernier, Domain wall motion by spin-polarized current: A micromagnetic study, *J. Appl. Phys.* **95**, 7049 (2004).
- [11] G. Tatara and H. Kohno, Theory of current-driven domain wall motion: Spin transfer versus momentum transfer, *Phys. Rev. Lett.* **92**, 086601 (2004).
- [12] W. Jiang, P. Upadhyaya, Y. Fan, J. Zhao, M. Wang, L.-T. Chang, M. Lang, K. L. Wong, M. Lewis, Y.-T. Lin, J. Tang, S. Cherepov, X. Zhou, Y. Tserkovnyak, R. N. Schwartz, and K. L. Wang, Direct imaging of thermally driven domain wall motion in magnetic insulators, *Phys. Rev. Lett.* **110**, 177202 (2013).
- [13] F. Schlickeiser, U. Ritzmann, D. Hinzke, and U. Nowak, Role of entropy in domain wall motion in thermal gradients, *Phys. Rev. Lett.* **113**, 097201 (2014).
- [14] P. Yan, Y. Cao, and J. Sinova, Thermodynamic magnon recoil for domain wall motion, *Phys. Rev. B* **92**, 100408(R) (2015).
- [15] S. K. Kim and Y. Tserkovnyak, Landau-Lifshitz theory of thermomagnonic torque, *Phys. Rev. B* **92**, 020410(R) (2015).
- [16] D.-S. Han, S.-K. Kim, J.-Y. Lee, S. J. Hermsdoerfer, H. Schultheiss, B. Leven, and B. Hillebrands, Magnetic domain-wall motion by propagating spin waves, *Appl. Phys. Lett.* **94**, 112502 (2009).
- [17] J. Han, P. Zhang, J. T. Hou, S. A. Siddiqui, and L. Liu, Mutual control of coherent spin waves and magnetic domain walls in a magnonic device, *Science* **366**, 1121 (2019).
- [18] Y. Fan, M. J. Gross, T. Fakhrlul, J. Finley, J. T. Hou, S. Ngo, L. Liu, and C. A. Ross, Coherent magnon-induced domain-wall motion in a magnetic insulator channel, *Nat. Nanotechnol.* **18**, 1000 (2023).
- [19] J. Lan, W. Yu, R. Wu, and J. Xiao, Spin-wave diode, *Phys. Rev. X* **5**, 041049 (2015).
- [20] W. Yu, J. Lan, and J. Xiao, Magnetic logic gate based on polarized spin waves, *Phys. Rev. Appl.* **13**, 024055 (2020).
- [21] X.-G. Wang, G.-H. Guo, Y.-Z. Nie, G.-F. Zhang, and Z.-X. Li, Domain wall motion induced by the magnonic spin current, *Phys. Rev. B* **86**, 054445 (2012).
- [22] W. Yu, J. Lan, and J. Xiao, Polarization-selective spin wave driven domain-wall motion in antiferromagnets, *Phys. Rev. B* **98**, 144422 (2018).
- [23] D. R. Rodrigues, A. Salimath, K. Everschor-Sitte, and K. M. D. Hals, Spin-wave driven bidirectional domain wall motion in kagome antiferromagnets, *Phys. Rev. Lett.* **127**, 157203 (2021).
- [24] P. Yan, X. S. Wang, and X. R. Wang, All-magnonic spin-transfer torque and domain wall propagation, *Phys. Rev. Lett.* **107**, 177207 (2011).
- [25] D. Hinzke and U. Nowak, Domain wall motion by the magnonic spin Seebeck effect, *Phys. Rev. Lett.* **107**, 027205 (2011).
- [26] M. Mochizuki, X. Z. Yu, S. Seki, N. Kanazawa, W. Koshibae, J. Zang, M. Mostovoy, Y. Tokura, and N. Nagaosa, Thermally driven ratchet motion of a skyrmion microcrystal and topological magnon Hall effect, *Nat. Mater.* **13**, 241 (2014).
- [27] H. Yu, J. Xiao, and H. Schultheiss, Magnetic texture based magnonics, *Phys. Rep.* **905**, 1 (2021).
- [28] E. G. Tveten, A. Qaiumzadeh, and A. Brataas, Antiferromagnetic domain wall motion induced by spin waves, *Phys. Rev. Lett.* **112**, 147204 (2014).
- [29] J. Lan, W. Yu, and J. Xiao, Antiferromagnetic domain wall as spin wave polarizer and retarder, *Nat. Commun.* **8**, 178 (2017).
- [30] A. Qaiumzadeh, L. A. Kristiansen, and A. Brataas, Controlling chiral domain walls in antiferromagnets using spin-wave helicity, *Phys. Rev. B* **97**, 020402(R) (2018).
- [31] S.-H. Oh, S. K. Kim, J. Xiao, and K.-J. Lee, Bidirectional spin-wave-driven domain wall motion in ferrimagnets, *Phys. Rev. B* **100**, 174403 (2019).
- [32] K.-W. Kim, H.-W. Lee, K.-J. Lee, and M. D. Stiles, Chirality from interfacial spin-orbit coupling effects in magnetic bilayers, *Phys. Rev. Lett.* **111**, 216601 (2013).
- [33] W. Wang, M. Albert, M. Beg, M.-A. Bisotti, D. Chernyshenko, D. Cortés-Ortuño, I. Hawke, and H. Fangohr, Magnon-driven domain-wall motion with the Dzyaloshinskii-Moriya interaction, *Phys. Rev. Lett.* **114**, 087203 (2015).

- [34] H. Ai and J. Lan, Anatomy of spin-wave-driven magnetic texture motion via magnonic torques, *Phys. Rev. B* **107**, 054441 (2023).
- [35] A. G. Gurevich and G. A. Melkov, *Magnetization Oscillations and Waves* (CRC Press, New York, 1990).
- [36] A. M. Kosevich, B. A. Ivanov, and A. S. Kovalev, Magnetic solitons, *Phys. Rep.* **194**, 117 (1990).
- [37] C. Kittel, *Introduction to Solid State Physics* (John Wiley & Sons, New York, 1953).
- [38] F. D. Stacey, The physical theory of rock magnetism, *Adv. Phys.* **12**, 45 (1963).
- [39] C. Dong, D. Guo, L. Wu, F. Wang, C. Jiang, C. Jia, and D. Xue, Piezoelectric control of magnetic anisotropy in the  $\text{Ni}_{0.46}\text{Zn}_{0.54}\text{Fe}_2\text{O}_4/\text{Pb}(\text{Mg}_{1/3}\text{Nb}_{2/3})\text{O}_3\text{-PbTiO}_3$  composite, *Appl. Phys. Lett.* **104**, 062403 (2014).
- [40] M. Ikhlas, S. Dasgupta, F. Theuss, T. Higo, S. Kittaka, B. J. Ramshaw, O. Tchernyshyov, C. W. Hicks, and S. Nakatsuji, Piezomagnetic switching of the anomalous Hall effect in an antiferromagnet at room temperature, *Nat. Phys.* **18**, 1086 (2022).
- [41] M. Liu and N. X. Sun, Voltage control of magnetism in multiferroic heterostructures, *Philos. Trans. R. Soc.* **372**, 20120439 (2014).
- [42] J. Zou, S. K. Kim, and Y. Tserkovnyak, Tuning entanglement by squeezing magnons in anisotropic magnets, *Phys. Rev. B* **101**, 014416 (2020).
- [43] R. Wieser, E. Y. Vedmedenko, and R. Wiesendanger, Domain wall motion damped by the emission of spin waves, *Phys. Rev. B* **81**, 024405 (2010).
- [44] X. S. Wang, P. Yan, Y. H. Shen, G. E. W. Bauer, and X. R. Wang, Domain wall propagation through spin wave emission, *Phys. Rev. Lett.* **109**, 167209 (2012).
- [45] J.-I. Kishine and A. S. Ovchinnikov, Adiabatic and nonadiabatic spin-transfer torques in the current-driven magnetic domain wall motion, *Phys. Rev. B* **81**, 134405 (2010).
- [46] J.-I. Kishine and A. S. Ovchinnikov, Theory of monoaxial chiral helimagnet, *Solid State Phys.* **66**, 1 (2015).
- [47] C. Cohen-Tannoudji, B. Diu, and F. Laloë, *Quantum Mechanics. Volume 1: Basic Concepts, Tools, and Applications* (Wiley-VCH, Weinheim, 2020).
- [48] J. Lan and J. Xiao, Spin wave driven domain wall motion in easy-plane ferromagnets: A particle perspective, *Phys. Rev. B* **106**, L020404 (2022).
- [49] G. E. Volovik, Linear momentum in ferromagnets, *J. Phys. C: Solid State Phys.* **20**, L83 (1987).
- [50] J. Lan and J. Xiao, Skew scattering and side jump of spin wave across magnetic texture, *Phys. Rev. B* **103**, 054428 (2021).
- [51] J. Lan, W. Yu, and J. Xiao, Geometric magnonics with chiral magnetic domain walls, *Phys. Rev. B* **103**, 214407 (2021).
- [52] F. D. M. Haldane, Geometrical interpretation of momentum and crystal momentum of classical and quantum ferromagnetic Heisenberg chains, *Phys. Rev. Lett.* **57**, 1488 (1986).
- [53] R. F. Egorov, I. G. Bostrem, and A. S. Ovchinnikov, The variational symmetries and conservation laws in classical theory of Heisenberg (anti)ferromagnet, *Phys. Lett. A* **292**, 325 (2002).
- [54] A. Auerbach, *Interacting Electrons and Quantum Magnetism* (Springer, New York, 1994).
- [55] P. Yan, A. Kamra, Y. Cao, and G. E. W. Bauer, Angular and linear momentum of excited ferromagnets, *Phys. Rev. B* **88**, 144413 (2013).
- [56] X.-G. Wang, L. Chotorlishvili, G.-H. Guo, A. Sukhov, V. Dugaev, J. Barnaś, and J. Berakdar, Thermally induced magnonic spin current, thermomagnonic torques, and domain-wall dynamics in the presence of Dzyaloshinskii-Moriya interaction, *Phys. Rev. B* **94**, 104410 (2016).
- [57] A. Donges, N. Grimm, F. Jakobs, S. Selzer, U. Ritzmann, U. Atxitia, and U. Nowak, Unveiling domain wall dynamics of ferrimagnets in thermal magnon currents: Competition of angular momentum transfer and entropic torque, *Phys. Rev. Res.* **2**, 013293 (2020).
- [58] A. Vansteenkiste, J. Leliaert, M. Dvornik, M. Helsen, F. Garcia-Sanchez, and B. Van Waeyenberge, The design and verification of MuMax3, *AIP Adv.* **4**, 107133 (2014).
- [59] A. A. Kovalev and Y. Tserkovnyak, Thermomagnonic spin transfer and Peltier effects in insulating magnets, *Europhys. Lett.* **97**, 67002 (2012).
- [60] W. Döring, Über die trägheit der wände zwischen weißschen bezirken, *Z. Naturforsch. A* **3**, 373 (1948).
- [61] L. Thomas, R. Moriya, C. Rettner, and S. S. P. Parkin, Dynamics of magnetic domain walls under their own inertia, *Science* **330**, 1810 (2010).
- [62] G. Pöschl and E. Teller, Bemerkungen zur quantenmechanik des anharmonischen oszillators, *Z. Phys.* **83**, 143 (1933).
- [63] A. A. Kovalev, Skyrmonic spin Seebeck effect via dissipative thermomagnonic torques, *Phys. Rev. B* **89**, 241101(R) (2014).
- [64] L. Landau and E. Lifshitz, *The Classical Theory of Fields*, Course of Theoretical Physics No. 2 (World Publishing Corporation, Beijing, 1990).
- [65] Z. Zhang, K. Lin, Y. Zhang, A. Bournel, K. Xia, M. Kläui, and W. Zhao, Magnon scattering modulated by omnidirectional hopfion motion in antiferromagnets for meta-learning, *Sci. Adv.* **9**, eade7439 (2023).